Geophys. J. Int. () , 1–8

Comparisons of surface wave amplitude decay for colocated rotation and translation measurements

Bryant Chow,[1⋆] Heiner Igel,[1] Joachim Wassermann,[1] Bernhard Schuberth,[1] Céline Hadziiannou,[1,2] and Stefanie Donner[1,3]

[1] *Department of Earth and Environmental Sciences, Ludwig-Maximilians-University Munich, Theresienstraße 41, D-80333 Munich, Germany.*
[2] *Department of Earth Science, University of Hamburg, Bundesstraße 55, D-20146 Hamburg, Germany*
[3] *Federal Institute for Geosciences and Natural Resources, Stilleweg 2, D-30655 Hannover, Germany*
E-mail: bryant.chow@vuw.ac.nz

SUMMARY
Current broad-band surface wave magnitude equations relate magnitude with station-receiver distance and the vertical component of peak ground velocity, such that only contributions from the vertical component of Rayleigh waves are present. With the advent of rotational ground motion data from instruments such as ring laser gyroscopes and fiber-optic gyroscopes, it is possible to determine peak amplitudes of rotations about the vertical axis, which is theoretically only sensitive to the transverse nature of Love waves, unaffected by the horizontal component of Rayleigh waves. We use this concept to study the amplitude decay of rotations versus translations, and determine the necessity of a separate surface wave magnitude equation for Love waves. Utilizing a large database of rotation ground motion events, collected in Wettzell, Germany, we empirically define decay constants for measured observables: rotation rate, rotation, vertical velocity and transverse velocity. Results indicate that measured rotation amplitudes decay faster over distance compared to velocity amplitudes, both on vertical and transverse components. Observations are corroborated with synthetic seismograms produced on a full scale 3D global model with crustal and Moho topography models. Synthetics were created with the spectral-element method Salvus, and suggest that ...

Key words: magnitude, rotational ground motions, seismic instrumentation, amplitude decay

1 INTRODUCTION

For over a decade, the application of ring laser gyroscope technology to the field of seismology has allowed for near-continuous, direct, measurements of rotational ground motions. An ever growing number of observations from seismic events of varying size, distance and source mechanism, has been collected in an expansive catalog of waveform recordings for both direct rotation, and collocated translation measurements. Previous work on this unique waveform dataset includes phase comparisons of translations and rotations with estimations of horizontal phase velocities [Igel 2005] automatic standardized processing of rotation and translation data [Salvermoser 2017], variations of surface wave energy in oceanic microseisms [Tanimoto ????],. [More citations here?] Much of this preceding work however, focuses on single events, or collections of non-earthquake sources. This paper, on the other hand, aims to utilize a large portion of the dataset.

In this paper, we aim to characterize and understand the differences in amplitude decay behavior of rotational and translational ground motion for a large number of seismic events. To do this, we make use of a sizable catalog of earthquake data, as measured by an observatory based ring laser gyroscope, and collocated broadband translation sensor. By processing rotation and translation observations in a near identical manner, we hope to directly compare results over a large set of event magnitudes, epicentral distances and azimuths. We additionally seek to use this information to better understand decay characteristics of Love and Rayleigh waves.

This paper builds on work previously addressed by Igel et al. 2007, where the question was posed: whether observed peak rotation amplitudes matched with expected values given by the surface wave magnitude equation. At the time, a limited number of recorded events lead to a small sample size. With a much larger number of events now currently available, we attempt to readdress this question, while also approaching the problem from the unique perspective of deriving magnitude scales to quantify and compare the decay characteristics of rotations and translations. Due to the uniqueness of our instrumental setup, we are restricted to observations at a single point of measurement. In order to provide comparisons to our observations, global 3D synthetic simulations were run with the wave propagation code Specfem3D Globe. Real seismic

⋆ Now at Victoria University of Wellington, School of Geography, Environment and Earth Sciences, Kelburn Parade, Wellington, New Zealand 6012 event locations, source parameters, and station locations are used, in order to provide the most comparable synthetic setup to observations.

With these observations, we aim to make quantitative statements on surface wave amplitude decay, as well as to provide magnitude scale equations that may prove useful in determining expected rotation amplitudes from seismic events.

1.1 Rotational Ground Motions

Rotational ground motions induced by seismic events can currently be observed through direct measurement, and through array analysis of translation sensors [Spudich ????]. In the latter, spatial gradients are taken for measurements in an adequately spaced array of translation sensors, in order to derive components of the strain tensor [Spudich ?]. A downfall of array based methods, however, is the necessity for multiple instruments with known calibrations, and the importance of array spacing and geometry in the clarity of the recorded signal. With unique instrument designs, however, direct gradient measurements are also possible [Schreiber? Others?].

Data for this study was recorded by the Großring (G-ring) [Schreiber 2005, 2006], a 4x4m helium-neon ring laser gyroscope, located in Wettzell, Germany (49.144°N, 12.87°E). The G-ring operates on the principle of Sagnac interferometry [Stedman, 1997], which relates interference of counter propagating light beams to absolute rotation rate, through the following equation,

$$\delta f = \frac{4A}{\lambda P}\mathbf{n}\cdot\mathbf{\Omega}, \tag{1}$$

where the constants are given by instrument area A, perimeter P and operating light wavelength λ. Equation 1 relates an observable beat frequency δf [Hz] to absolute rotation rate [rad/s] Ω.

It is important to note that given stable instrument geometry and lasing, changes to the beat frequency δf, can only be introduced by changes to the inner product of the plane normal $\mathbf{n}$ with the rotation rate direction $\hat{\mathbf{\Omega}}$ (e.g. through instrumental tilt), and through externally induced rotations (e.g. the passing of seismic waves). It has been shown that changes to the inner product as produced by tilt are one to two orders of magnitude smaller than rotations produced by passing seismic waves [Igel ????] [Schreiber ????], this provides unique benefit that G is theoretically insensitive to translations, and only sensitive to externally induced rotations.

1.1.1 Phase velocity relation

As shown in previous theoretical considerations towards measured rotations [Igel 2005], for a simple plane wave, the amplitudes of vertical rotation rate Ω_z and transverse acceleration $\ddot{u}_t$ can be related through the equation

$$\frac{\ddot{u}_t}{\Omega_z} = -2c, \tag{2}$$

where c represents an apparent horizontal phase velocity. This relationship shows that, given a sufficient event-receiver distance (allowing a plane wave assumption), measured rotations are sensitive to the transverse component of translation, represented in teleseismic waves by surface horizontal waves (i.e. SH or Love waves). It also shows that waveforms of transverse acceleration and vertical rotation rate should theoretically be in phase, with oppositely polarized amplitudes, for passing horizontal waves. This can be seen

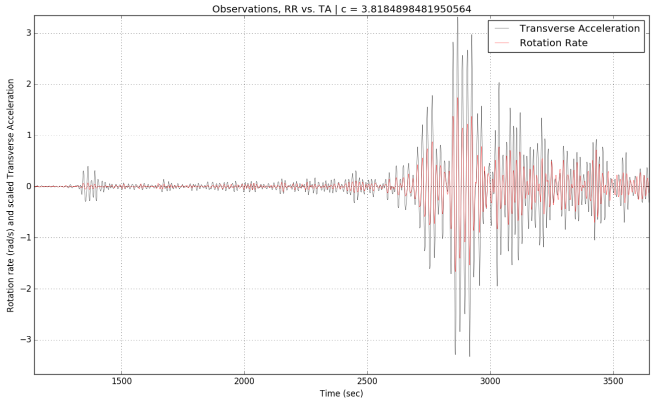

Figure 1. Teleseismic event filtered at dominant period 20s. Note the phase matching of transverse acceleration and rotation rate, as well as the calculated value of horizontal phase velocity, c=3.81 km/s.

in Figure 1, showing two superimposed traces of rotation rate and transverse acceleration (filtered at T=20 s) for G and a colocated broad band seismometer. Following Equation 2, a value of 3.81 km/s is calculated, which matches well with previous findings of phase velocity for this area [Igel 2007].

1.1.2 Peak correlation coefficient

Correlations are a useful measure of similarity between two signals. It has been shown previously that for collocated measurements of vertical rotation rate and transverse acceleration, high values ($>$ 0.9) of zero lag correlations can be obtained in time windows centered around surface wave arrivals. Zero lag correlation coefficients are routinely computed for events measured by G [Salvermoser 2017], and are used in this study as a filtering tool to highlight "bad" events that exhibit low signal to noise ratios, or dissimilar waveforms which may arise due to non-physical effects (e.g. instrumental effects). Here, the largest correlation coefficient obtained for a seismogram is labeled the peak correlation coefficient (PCC), and is used as a representation of data quality for an event.

1.2 Magnitude scales

Here we discuss the common magnitude scale equation, and propose using a modified version of the equation as a method for comparing amplitude decay of various observables. Amplitude based magnitude scales provide empirically derived relationships between maximum trace amplitudes and source-receiver distances. Magnitude scales offer useful and quick estimates of relative sizes of earthquakes in a simple, standard manner. The International Association of Planets Seismology and Earths Interior (IASPEI) Working Group on Magnitudes proposed a modified version of the original surface wave magnitude equation proposed by Karnik et al. and Vanek et al., which is compatible for use with modern day broadband seismic instruments [Borrmann & Bergman 2000].

In this work, we adhere strictly to these standard procedures provided by IASPEI as an outline for defining our own empirical magnitude scales. In turn, we use these derived scales as a tool for quantifying amplitude decay for different measured observables.

1.2.1 Standard Procedures

The Working Group on Magnitudes' standard procedures gives the revised surface wave magnitude equation for broad-band instruments as,

$$M_S^{BB} = log_{10}(V/2\pi) + B \cdot log_{10}(\Delta) + C, \tag{3}$$

where the constants $B = 1.66$ and $C = 0.3$ control amplitude decay and order of magnitude, respectively. The parameter V should be the maximum trace amplitude (in nanometers second^{-1}) in the surface wave train, for a seismogram proportional to velocity, measured on the vertical component.

Further criteria given by IASPEI posit that the period of the surface wave should lie within 3 s $\leq$ T $\leq$ 60 s, while epicentral distances should be between $2^\circ \leq \Delta \leq 160^\circ$. It is further recommended that only shallow focus earthquakes should be considered, as medium to deep events are less capable of generating strong surface waves. Maximum trace amplitudes are described as one half the largest peak to adjacent trough deflection, and associated period are given as two times the temporal difference between peak and adjacent trough. All events and processing steps in this paper adhere to these guidelines.

1.2.2 Instrumental proxies for Love and Rayleigh waves

A standard procedure for determining surface wave magnitude scales is to take amplitudes measured on the vertical component of translation. This is because vertical translation should only be sensitive to the vertical motions of Rayleigh waves, whereas vector sums of horizontal components can be influenced by both Love and Rayleigh waves. In the same vein, velocity measured on the transverse component should only show sensitivity to Love waves (and radial components should only be sensitive to the horizontal component of Rayleigh waves). This is, however not common practice, due to the necessity of rotating horizontal components to the correct azimuth, which can be affected by ray paths and local site effects. The G-ring, which is: 1) insensitive to translations and 2) proportional in phase and amplitude to transverse acceleration, should however only be sensitive to Love waves in the surface wave train, irrespective of azimuth.

In this study we use our instruments as physical wave-filters, in order to separate phases in the surface wave train. This allows us to study the influences of Love waves and Rayleigh waves individually. By comparing the vertical and transverse components of translations, to the vertical component of rotation, we can understand, by proxy, the wave types they are sensitive to.

1.2.3 Application of rotations to magnitude scales

The surface wave magnitude equation is defined for peak vertical velocity amplitudes in the surface wave train. In order to give a fair comparison using derived magnitude scales, a complementary rotation parameter is necessary. In Section 1.1.1, an equation is given that relates rotation rates Ω with accelerations $\ddot{u}$. It would make the most sense, then, to compare velocities $\dot{u}$ with rotations ω (by integrating both sides). However, without previous work to draw precedence from, and for completeness, we present observations of both rotations and rotation rates in this study.

2 EVENT CHOICE

The G-ring has been continuously recording at its current resolution since May, 2009 [Citation for mirror upgrade?]. The time range for events used in this study spans June 1, 2009 to September 1, 2016. An initial earthquake catalog was fetched from the Harvard Global Centroid Moment Tensor (GCMT) [Ekström et al. 2012 ?], with events filtered by acceptable magnitude, source depth and epicentral distance from Wettzell, Germany. At this point we imposed the restriction that the derived 'magnitude' as given by our magnitude equations, should fall as close to the given surface wave magnitude as possible. This ensures that our derived scales do not stray too far from established scales. This meant that only events with centroid moment magnitude values of $6 \leq M_{\mathrm{wc}} < 8$ (as published in the GCMT catalog), were considered; surface wave magnitude and moment magnitude are approximately equal in this range [Shearer 2009]. Zero-lag cross correlations of transverse acceleration and rotation rate were taken in order to calculate peak correlation coefficients (Section 3.1). Events were not considered if their peak correlation coefficient did not meet the criterion PCC < 0.7.

These choices for event criteria narrowed the catalog down to roughyl 500 events in the given time period. Each event was appropriately filtered and processed (Section 3.1), and waveforms were individually inspected. Waveforms that exhibited anomalous behavior (i.e. unexpected high amplitude peaks outside the surface wave train, high signal-to-noise ratio etc.) were rejected. A final event catalog of 243 events was reached, shown on a world map in Figure 2.

3 METHODS

3.1 Data Processing

Events were processed in a similar fashion as the processing outlined in Salvermoser 2017. Raw, continuous translation data in North, East and vertical components, as well as vertical rotation rate data, was fetched based on event origin time. Instrument response correction produced translation seismograms proportional to units of velocity (nm s^{-1}). Epicentral distances (Δ) and theoretical backazimuth values were calculated from station-receiver latitude longitude pairs, and events were separated into categories of close ($\Delta < 3^\circ$), local ($\Delta < 100^\circ$) and far ($\Delta \geq 100^\circ$). Horizontal components were rotated into the transverse, radial, vertical coordinate system by the appropriate theoretical backazimuth. Measurements from ring laser gyroscope instruments do not require frequency dependent instrument correction [Sagnac ????], therefore only a simple scale factor was necessary to retrieve seismograms proportional to rotation rate (nrad s^{-1}). Rotation rate traces were integrated to provide measurements of rotation (nrad), and transverse velocity was integrated to retrieve transverse acceleration, which was subsequently used to calculate correlations with vertical rotation rates. A bandpass filter was applied to all traces for periods between 3 s $\leq$ T $\leq$ 60 s, in accordance to the IASPEI standard procedures. Peak amplitudes were chosen by finding minimum and maximum trace values and the largest associated peak or trough, respectively. The larger of the two was chosen, alongside the associated arrival time and dominant period, taken as two times the distance between peak and adjacent trough. Theoretical considerations used to restrict search to the surface wave train proved inconsistent over a large number of events, so maximum amplitudes in the entire trace were considered. Through manual inspection, picked amplitudes that fell outside the surface wave train (which occurred very

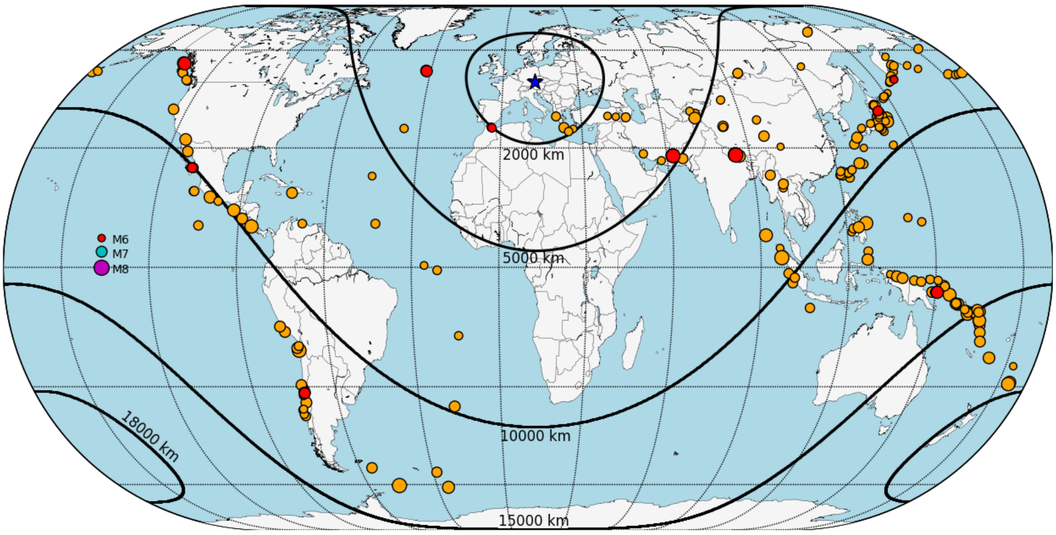

Figure 2. Event map. Size represents moment magnitude (M$_{wc}$). Orange dots show observed earthquakes used in magnitude scale derivation. Red dots show the ten events chosen for generation of synthetic seismograms. Black lines are equidistant points from the blue star, which represents the location of G in Wettzell, Germany (49.144°N,12.87°E).

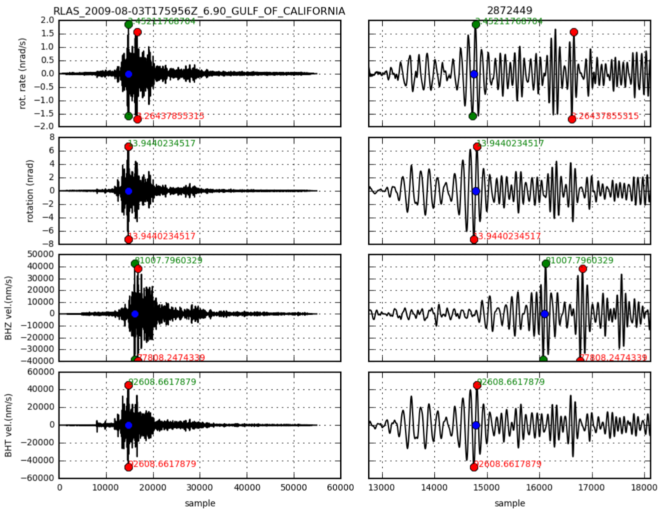

Figure 3. Left: Seismograms for observed rotation rate, rotation (measured by G), and two components of translation (colocated STS-2), vertical and transverse components.
Right: Zoomed in section of seismograms, showing peak to peak amplitude choice (blue dot). Red and green dots show largest peak to adjacent trough distance and largest trough to adjacent peak distance, respectively. Note the visible difference in arrival times of the Love wave (as seen on rotation and transverse components), and the later arriving Rayleigh wave (as seen on the vertical component).

infrequently) were rejected. An example of the waveforms and amplitude picking is shown in Figure **??**.

3.1.1 Zero-lag correlations

To calculate peak correlations, traces of transverse acceleration and vertical rotation rate were segmented into small time windows based on the event-station distance. In each time window, a zero-lag correlation was performed, and a single value of correlation produced. From the entire trace, the max value was taken to represent the peak correlation coefficient. For most waveforms, the peak correlation coefficient lie in the surface wave train. As mentioned previously, these peak correlation values are used extensively as a ranking system for events, providing a quickly attainable measure of waveform quality.

3.2 Curve fitting

To quantify amplitude decay, magnitude scale coefficients were fit to the data using a simple linear regression. Equation 3 represents a relationship between magnitude and amplitude for a single event. Using Equation 3, a collection of n events can be represented in the form,

$$\begin{pmatrix} log_{10}(\Delta_1) & 1 \\ log_{10}(\Delta_2) & 1 \\ \vdots & \vdots \\ log_{10}(\Delta_n) & 1 \end{pmatrix} \begin{pmatrix} B \\ C \end{pmatrix} = \begin{pmatrix} M_{\mathrm{wc}_1} - log_{10}(V_1/2\pi)_{\max} \\ M_{\mathrm{wc}_2} - log_{10}(V_2/2\pi)_{\max} \\ \vdots \\ M_{\mathrm{wc}_n} - log_{10}(V_n/2\pi)_{\max} \end{pmatrix}, \tag{4}$$

which can be further condensed to the form, $\mathbf{Gm} = \mathbf{d}$. The unknowns B and C are represented in the vector $\mathbf{m}$, and can be solved for through the normal equation $\mathbf{m} = (\mathbf{G}^T\mathbf{G})^{-1}\mathbf{G}^T\mathbf{d}$. By determining values of B and C, we create an empirical magnitude scale that best describes the amplitude decay behavior of our events. In Equation 4, we impose that our derived magnitude value should be as close to an events given moment magnitude as possible, by setting M_S^{BB} equal to the value of M_{wc} retrieved from our event catalog.

95% confidence intervals were constructed for each parameter of the vector $\mathbf{m}$. These were calculated with the variance of estimates of the jth parameter of $\mathbf{m}$ by the equation $\hat{m}_j \pm c\sqrt{\hat{var}(\hat{m}_j)}$, where the value of c is given as 1.96 for a confidence interval of $\alpha = 0.95$.

4 SYNTHETIC SEISMOGRAMS

Due to the unique instrumental setup of the G-ring, there are currently no other rotational instruments with as much temporal coverage to draw comparisons from. It should be mentioned that there are other available rotation instruments which allow for single event case study analyses [Donner 2017 PFO?] [iXblue?] [PFORLAS], however large catalogs like that available from the G-ring are currently unavailable. One possibility for gathering more observations would be through array derived rotations as a substitute for direct rotation measurements [Spudich ?]; this option was noted during analysis, however it proved difficult finding sufficient long-term arrays with the optimal station spacing. In the future if this type of data became available, it would provide a very useful addition of information to this study. In lieu of observations, we instead turn to waveform modeling to generate synthetic seismograms, with which we recreate our experimental setup and provide a comparable set of synthetic observations.

The seismic wave propagation code Specfem3D Globe was employed [cite specfem]. A realistic global model featuring 3D crust and mantle models was used, and the simulation featured effects that might have potential influence on surface waves at the periods of interest. These effects include: ocean loading, Earth's ellipticity, topography, self gravitation, Earth's rotation and 1-D attenuation. Event locations and moment tensors were taken from 10 real seismic events present in the observation catalogs. Events were chosen based on observation data quality, as well as event location and depth, so as to provide a varied distribution of source-receiver pairings. Table 1 provides detailed information on the chosen events.

In each simulation, events were initiated as point sources. The simulation corner frequency was set to 10 seconds, and simulations were run for one hour simulation time. As computational cost is independent of number of stations, more than one hundred stations were included; Global Seismic Network (GSN) locations were used, as well as location of the G-ring, and the German observatory station Fürstenfeldbruck. The number of simulated stations was X, and the number of station-receiver pairs X (with some station-receiver pairs falling outside the distance bounds specified in Section 1.2.1).

The direct outputs of Specfem3D were adjusted to produce displacement (in units of meters) in the transverse, radial and vertical components, by rotation with respect to the theoretical backazimuth. Direct rotation (in units of radians) in the same coordinate system was also outputted. During processing, translation seismograms were differentiated to retrieve velocity waveforms, and rotation was differentiated to produce rotation rate waveforms. A work flow identical to that used for observations was employed to calculate peak trace amplitudes, and a magnitude equation was fit to the data for comparison.

5 RESULTS

5.1 Derived magnitude scales

Decay characteristics of rotations and translations were derived by solving for constants B and C in Equation 4. The values for each scale are presented in Table 2. For additional quality control on the processing steps, and on site-dependent data quality, the same analysis was performed on translation observations taken at the geophysical observatory Fürstenfeldbruck, Germany (FUR; 48.163°N, 11.275°E), located roughly 200 km south-west of Wettzell. Though a smaller subset of events was used due to data availability, the results confirmed those given by Wettzell.

Table 2 shows that the value of B covers a large range of values, ranging from 1.084 to 1.823 for vertical velocity M_Z^{WET} and rotation rate M_{RR}^{RLAS}, respectively. Rotation M_{RT}^{RLAS} falls closest to the standard IASPEI value of B, 1.66. Velocity values match quite consistently between Wettzell and Fürstenfeldbruck, with FFB showing slightly higher amplitudes, as seen in the value of C, which controls the order of magnitude of each magnitude scale. Consideration should be given to the subsurface composition of WET and FUR; the geodetic observatory in Wettzell overlies granitic bedrock, while Fürstenfeldbruck sits atop a sedimentary basin. It is therefore expected that we should observe on-average larger amplitudes at Fürstenfeldbruck, due to basin amplification effects. This is visible in the transverse component, sensitive to Love waves, in Figure 6, however the vertical component, sensitive to the vertical component of Rayleigh waves, does not reflect this.

Variations of velocity based scales from the surface wave magnitude equation are large, however not as unsurprising as they first appear. In previous literature, it has been proposed that the modern surface wave magnitude equation has a systematic distance bias, which tends to under predict amplitudes at greater distances [Herak Herak 1993]. Previous works have proposed corrected values of the coefficients B and C, for a global catalog [Herak Herak 1993] and a European region dataset [Ambraseys Free 1997]. These corrections match well with the vertical velocity scales derived in this work; the values (adjusted for the change of units in the IASPEI scale) are presented in Table 2 as M_S^{HH} and M_S^{AF} for scales proposed in Herak Herak 1993 and Ambraseys-Free 1997, respectively.

There also exists a noticeable difference between values of B for transverse and vertical velocities. As the surface wave magnitude equation is defined for vertical component observations, the vertical velocity scale presents an identical setup as the broadband surface wave magnitude equation, however it gives here with the largest discrepancy, for both stations WET and FUR. Transverse velocity, which should sample Love waves, same as rotations (see 1.2.2), shows a larger value for B as compared to vertical velocity, however it also exhibits lower than expected decay compared to the IASPEI scale.

It is to be expected that rotation rate shows a larger value for B as compared to rotation, as rotation is being compared with its time derivative, which contains amplified high frequency components and should exhibit faster decay with distance as the wave path filters out this high frequency energy.

Confidence intervals, which can be viewed as a quantification of misfit between the fitted magnitude equation and the observations, shows the uncertainty of the observations due to the limitation of spatial coverage; in Figure 4, the red shaded area shows the confidence interval of the magnitude 6 decay line. It should be noted that the magnitude scale is heavily controlled by the end members at very close and far distances. Due to a lack of events at very close epicentral distances, it is difficult to constrain the decay here, and the few events that are at distances less than 20° have a strong influence on the derived value of B. It can also be seen that more than one third of the events used in this study fall around 80° epicentral distance, due to geographic constraints. Many of these events occur around Japan, and provide a good constraint of amplitudes at this distance.

Date	Time (UTC)	Lat(°)	Lon(°)	Depth(km)	M_{wc}	Flinn-Engdahl Region	Peak Corr. Coeff.
2010-07-18	13:34:59	-5.93	150.59	35.0	7.32	New Britain Region, P.N.G.	0.98
2011-09-16	19:26:41	40.27	142.78	35.0	6.67	Off East Coast Of Honshu, Japan	0.99
2013-01-05	08:58:19	55.39	-134.65	10.0	7.53	Southeastern Alaska	0.95
2013-04-16	10:44:20	28.03	62.0	80.0	7.74	Southern Iran	0.98
2013-04-19	19:58:40	49.97	157.65	15.0	6.06	East Of Kuril Islands	0.99
2015-02-13	18:59:12	52.65	-31.9	16.7	7.07	Reykjanes Ridge	0.99
2015-04-25	06:11:26	28.15	84.71	15.0	7.88	Nepal	0.99
2015-09-13	08:14:12	25.14	-109.43	10.0	6.6	Gulf Of California	0.98
2015-09-16	23:18:41	-31.56	-71.43	28.4	7.1	Near Coast Of Central Chile	0.99
2016-01-25	04:22:02	35.65	-3.68	12.0	6.38	Strait Of Gibraltar	0.99

Table 1. List of events used as synthetic sources in Specfem3D. Peak correlations are used as a measure of waveform quality, and only events with the highest values were used, in order to provide the best comparisons of synthetics with observations. Events were also chosen based on a diverse coverage of magnitudes and epicentral distances from the ring laser stationed in Wettzell, Germany. Event information taken from the GCMT catalog.

5.2 Observed and synthetic waveforms

For each of the simulated events, synthetic seismograms were generated for all synthetic stations mentioned previously. Waveforms for station WET were compared for all possible components of translation and rotation. In one event (2010-07-18), a fore shock in the observations, which went unnoticed during event choice, obscured body wave arrival times and made comparison difficult/impossible. In most other cases, P-wave and S-wave arrivals matched well. Later arrivals are not in agreement with very different behavior exhibited by arriving surface waves. This can be potentially explained by the use of point sources for such large magnitude earthquakes; the effects of the source time function as well as the rupture plane are not captured in our synthetics, and we therefore do not expect to match phases of surface wave arrivals. Consideration should also be given to the topographic and crustal models included, which affect the resulting surface wave waveforms. Fortunately we focus on peak amplitude measurements in this work, and therefore are not deterred by the misfit of waveforms. The broad frequency range (10-60s) also present difficulties in matching waveforms. Narrow pass filters (i.e. 20 second dominant period) capture similarities much better, however in this study we aim to stick to the definition of the IASPEI surface wave magnitude equation.

As to be expected, the observed waveforms present a much more complicated picture of arrivals. In most of the observations, noise levels are high enough that determining body wave arrivals is difficult compared to the synthetic models. Even for narrow pass filters, as in Figure 7, observation and synthetic seismograms do not exhibit high correlations. Neverthless, peak amplitude picking in all 10 events falls in the surface wave train which allows for determination of magnitude scales - this allows us to make comparisons without relying on waveform information.

Comparisons of transverse acceleration and rotation rate provide solid phase matching throughout the waveform, with the strongest correlation during the surface wave train, even for relatively wide bandpass filters (i.e. 10 to 60 seconds). This is true for both observations and synthetics, and also allows for the calculation of phase velocities. Because this is not the goal of this paper, we do not delve too far into the analysis of phase velocities, however taking peak value amplitude ratios for broad bandpass filter ranges (which would average the horizontal phase velocities of each dominant period contained), we recover values ranging from 3 to 5 km/s.

5.3 Synthetic magnitude scales

The derived magnitude scales for synthetic results are given in Table 2, with a figure showing the synthetic rotation rate magnitude scale in Figure 8. Looking at Table 2, the synthetic results vary quite dramatically from the observed results; the synthetic results do not reflect the same discrepancies that are present in the values given in Table 2.

Looking at Figure 8, the distribution of points on the magnitude scales is much more uniform. This can be attributed to the increased number of recordings for a single event due to the large number of synthetic stations. With so many station receiver pairs over a range of epicentral distances, the synthetic magnitude scale simulates the much more common method of determining magnitude. The number of events is roughly six times more than in observations, although the number of events at very close distances is also quite low, due to geographic considerations. The 95% confidence intervals provide a much narrower band than seen in observations, due to the larger number of events and the synthetic nature of this scale; single events providing data points over the entire distance range puts a strong constraint on the fitted decay constants.

The synthetic magnitude scales all exhibit very similar values for the decay constant B. The large variation in decay as seen in the observations is not captured here. Compared to the IASPEI magnitude scale, all the synthetic scales fall much lower in their value of B. Synthetic rotation rate gives the largest, or steepest decay constant at 1.215, however not by a large margin. Transverse velocity falls in with the smallest value. Looking at the values of C, expected amplitudes are all also quite low, except for rotation rate. Vertical velocity exhibits a n

5.4 Expected rotation amplitudes

One useful aspect of magnitude scales is to provide an expected amplitude value for a given magnitude event at certain distance. This is quite helpful in areas such as seismic hazard, where one can estimate the order of magnitude of ground motion at a location some distance away from an event, given a certain event size, though this is also dependent on many factors, such as site effects, travel paths, and amplitude modulation due to attenuation, focusing etc. This has largely been replaced by the concept of ground motion prediction equations, however it still provides a useful insight.

One concern in rotational seismology arises from whether or not newly developed field deployable rotation sensors can reach the sensitivity necessary to capture the rotational motion amplitudes

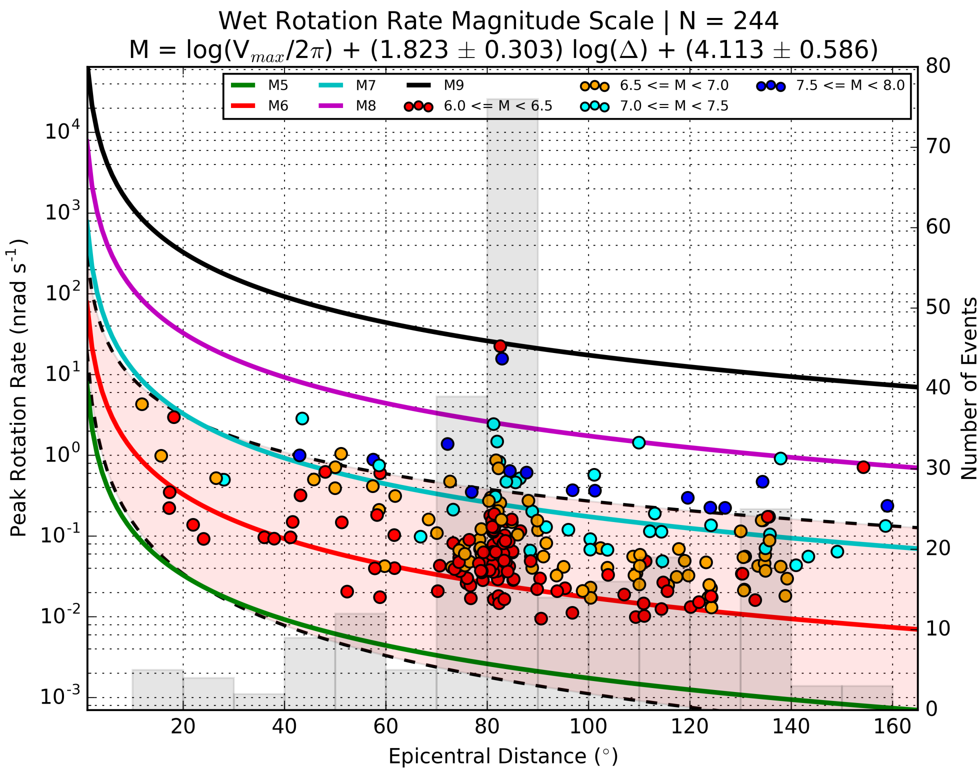

Figure 4. Rotation rate magnitude scale for observations. Event magnitudes separated by bins of 0.5 and denoted by color. Magnitude equation plotted by integer values as solid color lines. 95% confidence interval for M6 shown by the shaded red area, bordered by black dashed lines. The number of events for each epicentral distance bin shown by gray bars in the background.

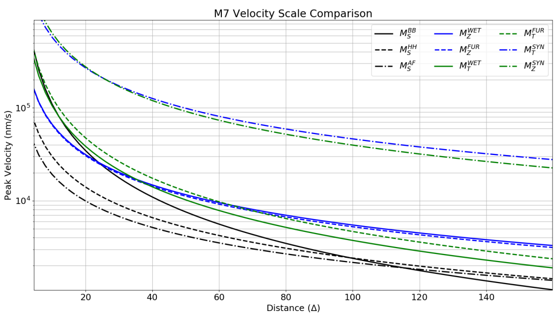

Figure 5. A comparison of velocity based scales for stations WET, FUR and synthetic scales, with the IASPEI scale used as reference. Peak amplitudes given in units of nanometers/s

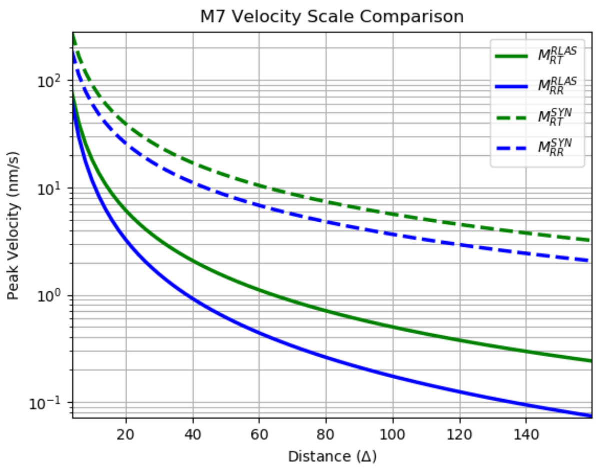

Figure 6. A comparison of rotation based scales for station WET and synthetic scales. Peak amplitudes given in units of nanoradians/s

excited by regional or tele- seismic events. With the rotational magnitude scale derived here, we are able to create a list of observation based expected amplitudes. At the time of writing, the field deployable rotation sensor BlueSeis from the company iXBlue, has a noise floor of roughly 1 nrad/s/$\sqrt{Hz}$ [Cite iXBlue]. Referring to the values of B and C for rotation rate given in Table 2, the maximum distance the sensor can be placed to detect a M_w5 event would be 21° epicentral distance, roughly 2000 km. This distance range would mean current day sensors could detect regional ¿M5 earthquakes. Other considerations must be taken into account before these values can be used for field deployment decisions, however it provides a jumping off point for this new area of field research.

6 DISCUSSION

The long term continuous recordings of colocated rotation and translation waveforms currently provides an extensive catalog of observations with which it is possible to explore seismic signals for events of varying source parameters, including magnitude, moment tensor, epicentral distance etc.

The motivation for addressing amplitude decays in the initial

Scale	Label	B	C	Wave
IASPEI	M_S^{BB}	1.66	0.3	Rayleigh
Herak Herak 1993	M_S^{HH}	1.094	1.429	Rayleigh
Ambraseys-Free 1997	M_S^{AF}	0.947	1.77	Rayleigh
Rotation	M_{RT}^{RLAS}	1.557 ± 0.295	4.186 ± 0.569	Love
Rotation Rate	M_{RR}^{RLAS}	1.823 ± 0.303	4.113 ± 0.586	Love
Transverse Velocity (Wettzell)	M_T^{WET}	1.45 ± 0.27	0.527 ± 0.521	Love
Transverse Velocity (FFB)	M_T^{FUR}	1.442 ± 0.27	0.447 ± 0.523	Love
Vertical Velocity (Wettzell)	M_Z^{WET}	1.084 ± 0.264	1.093 ± 0.511	Rayleigh
Vertical Velocity (FFB)	M_Z^{FUR}	1.095 ± 0.259	1.09 ± 0.502	Rayleigh

Table 2. Magnitude scales and derived constants with 95% confidence intervals for observations at instruments RLAS, WET (Wettzell, Germany) and FUR (Fürstenfeldbruck, Germany), for equations of the form $M = log_{10}(V/2\pi) + B \cdot log_{10}(\Delta) + C$. The final column gives consideration to the wave type that each instrument component should provide a proxy for.

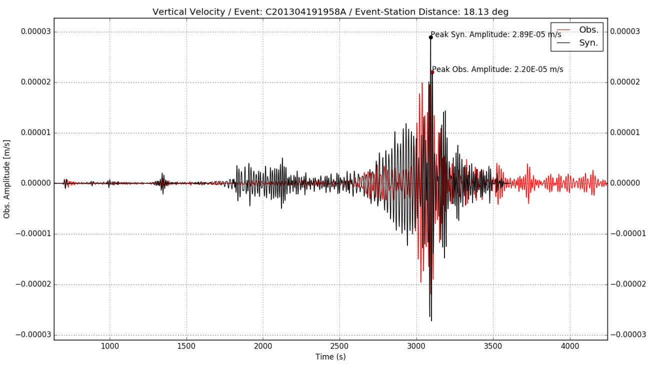

Figure 7. A comparison of synthetic and observed waveforms for an M6.1 event, East of Kuril Islands. Waveforms filtered at dominant period 20s.

study of Igel et al. 2007, was to determine whether or not the peak observed rotation rates were consistent with the definition of the surface wave magnitude equation. In this study we expanded our motivation to include the comparison of decay rates between rotations and translations, to see if and how these quantities differed. The question posed proves very interesting as measurements of seismically induced rotation amplitudes have not been addressed on such a scale before. If rotations are to be incorporated into standard seismological practices, it is useful and beneficial to understand these characteristics.

The findings of this study paint an interesting picture of both rotation and translation peak amplitudes.

Comparisons with the IASPEI scale should be taken with caution however. This broadband scale was devised by Karnik et al and Vanek et al. as a global averaging of magnitudes. Because of this, all local and regional effects from these scales are included in the averaging, which would present a difference in setting as compared to the single station derivation that is performed in this study. However, regardless of the number of stations, the magnitude scale should be a generally applicable equation that only relates distance with peak amplitude as a function of magnitude. The large degree of variation between the IASPEI scale and vertical velocity found in this study have been addressed in previous publications; Herak & Herak (1993) as well as Ambraseys-Free (1997) both concluded that there may be a distance bias in the surface wave magnitude equation, and they proposed new magnitude scales which match quite closely to the value of M_Z^{WET} determined here. These studies do not go into the effects of Love waves on this scale however, which is captured both by rotations and transverse velocity. Velocity in the transverse direction is susceptible to the azimuth of the event and how the components of the transverse component are rotated, however it paints a clear picture that decay is faster for velocity measured in the transverse component as compared to the vertical. Looking at Figure 6, we can see that this would lead to amplitude differences a factor of 4 different at epicentral distances of 80°, which is the most sampled distance in our observations.

to add: -structure differences between ffb and wettzell -high frequency attenutation of rotation rate compared to rotation -herak and herak newly proposed magnitude scale -averaging of earth structure not done here -considerations towards using the correct backazimuth -confidence interval -because of the logarithmic nature of magnitude scales, even differences in the decay constant don't make that much of an impact on the resulting expected amplitudes that one sees -using the same value of c for all rotation, at 80 degrees you get an order of magnitude difference in expected amplitude for synthetic and observed scales -because we use Mw and therefore Ms as a controlling parameter in our linear regression, it has a strong effect on the end result for our fitted line -large earthquakes being approximated as point sources with boxcar-like source time functions - not capturing the effects of the rupture so we aren't matching wiggle by wiggle. Even then we are consistently over predicting amplitudes

misc: how to convert from old magnitude scales to new - just subtract 3 from C (rewriting of magnitude equation)

+ considerations for observations and synthetics - geographical, data, frequency wise + observation results by themselves + synthetic results by themselves + comparisons of observations and synthetics + questions that arose from the processing + further work

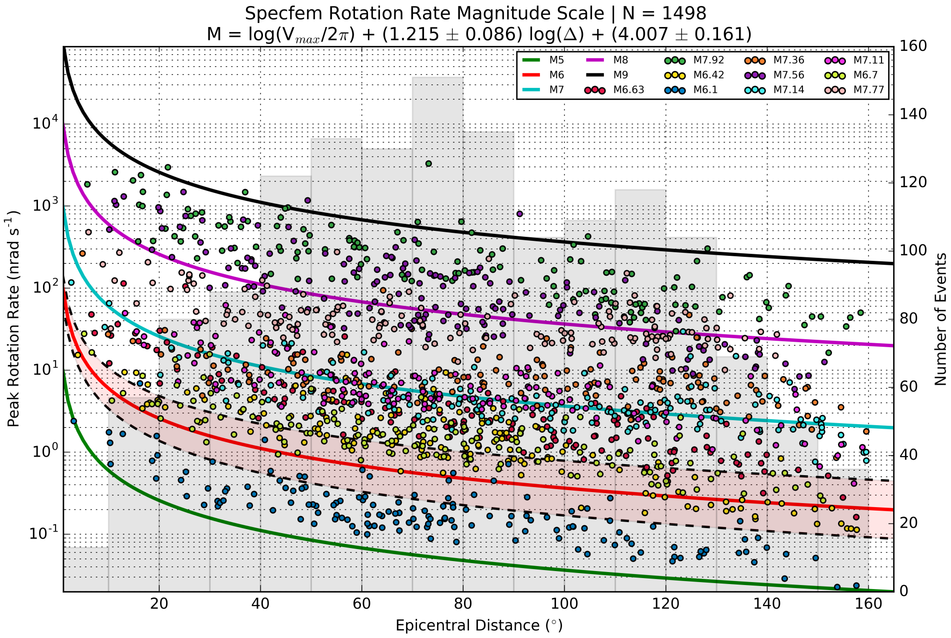

Figure 8. Rotation rate magnitude scale for synthetics. All objects similarly represented as in Figure 4. Colors of points here represent individual events simulated (for event information, see Table 1).

Scale	Label	B	C	Wave
Synthetic Rotation	M_{RT}^{SYN}	1.204 ± 0.086	3.841 ± 0.159	Love
Synthetic Rotation Rate	M_{RR}^{SYN}	1.215 ± 0.086	4.007 ± 0.161	Love
Synthetic Transverse Velocity	M_{T}^{SYN}	1.094 ± 0.081	0.146 ± 0.16	Love
Synthetic Vertical Velocity	M_{Z}^{SYN}	1.206 ± 0.08	-0.011 ± 0.149	Rayleigh

Table 3. Synthetic magnitude scales and derived constants with 95% confidence intervals, for equations of the form $M = log_{10}(V/2\pi) + B \cdot log_{10}(\Delta) + C$. The final column gives consideration to the wave type that each instrument component should provide a proxy for.